

*Supporting Information (SI) for*

## **High-temperature negative thermal quenching phosphors from molecular-based materials**

Huixian Miao,<sup>†a</sup> Yujie Zhou,<sup>†b</sup> Pingping Wang,<sup>a</sup> Zetao Huang,<sup>a</sup> Wenjiang Zhaxi,<sup>a</sup> Luying Liu,<sup>a</sup> Fengnan Duan,<sup>a</sup> Jinmin Wang,<sup>a</sup> Xiao Ma,<sup>a</sup> Shenlong Jiang,<sup>b</sup> Wei Huang,<sup>\*a</sup> Qun Zhang,<sup>\*b,c</sup> and Dayu Wu<sup>\*a</sup>

<sup>a</sup>Jiangsu Key Laboratory of Advanced Catalytic Materials and Technology, Advanced Catalysis & Green Manufacturing Collaborative Innovation Center, School of Petrochemical Engineering, Changzhou University, Changzhou, Jiangsu 213164, P. R. China. E-mail: wudy@cczu.edu.cn; whuang@cczu.edu.cn

<sup>b</sup>Hefei National Research Center for Physical Sciences at the Microscale, Department of Chemical Physics, University of Science and Technology of China, Hefei, Anhui 230026, P. R. China. E-mail: qunzh@ustc.edu.cn

<sup>c</sup>Hefei National Laboratory, University of Science and Technology of China, Hefei, Anhui 230088, P. R. China.

<sup>†</sup>These authors contributed equally to this work.

## Experimental Section

**Materials and General Procedures.** All chemicals and reagents were purchased from Aldrich and used as received without further purification. The ligands of bimb and bmimb were prepared according to the literature methods.<sup>1</sup>

### Synthesis of 1,2-bis((1H-imidazol-1-yl)methyl)benzene (bimb)

A solution containing imidazole (3.16 g, 46.4 mmol) and  $\alpha,\alpha'$ -dichloro-o-xylene (0.78 g, 4.46 mmol) in methanol (50 mL) was heated under reflux for 20 hours at 80 °C. After cooling at RT, the solvent was evaporated under reduced pressure and yellow syrup resulted, which was then dissolved in 80 ml aqueous potassium carbonate (6.13 g). The resulting solution was left undisturbed to produce large crystals which were identified as product (Fig. S1). Yield: 1.0 g (82%). <sup>1</sup>H NMR (400 MHz, CDCl<sub>3</sub>)  $\delta$  7.49 (s, 2H), 7.41 (dd, J = 4.6, 2.7 Hz, 2H), 7.29 (s, 2H), 7.14 (dd, J = 4.6, 2.7Hz, 2H), 6.82 (s, 2H), 5.06 (s, 4H).

### Synthesis of 1,2-bis((2-methyl-1H-imidazol-1-yl)methyl)benzene (bmimb)

The synthesis of bmimb followed the similar procedure to that of bimb except using 2-methylimidazole instead of imidazole. Yield: 80%. <sup>1</sup>H NMR (400 MHz, CDCl<sub>3</sub>)  $\delta$  7.36 (dd, J = 5.6, 3.2 Hz, 2H), 7.03 (s, 2H), 6.87 (dd, J = 5.6, 3.2 Hz, 2H), 6.73 (s, 2H), 4.99 (s, 4H), 2.35 (s, 6H).

### Synthesis of [(bimb)<sub>2</sub>Cu<sub>4</sub>I<sub>4</sub>]<sub>n</sub> (CP1)

A mixture of CuI (38 mg, 0.2 mmol), bimb (17.1 mg, 0.08 mmol), and CH<sub>3</sub>CN (2 mL), H<sub>2</sub>O (6 mL) was sealed in a 15 mL Teflon-lined autoclave, which was heated at 180 °C for 3 days. After slowly cooling to RT, the pale yellow crystals suitable for X-ray diffraction analysis were obtained, which were washed with distilled water and acetonitrile several times, and finally dried in air. Yield: 65% based on bimb. Infrared (IR) analysis (KBr, cm<sup>-1</sup>): 628(w), 656(s), 736(s), 823(m), 939(w), 1030(w), 1080(s), 1110(s), 1230(s), 1280(w), 1360(w), 1430(w), 1520(s). (Fig. S2) Anal. Calcd for C<sub>28</sub>H<sub>28</sub>Cu<sub>4</sub>I<sub>4</sub>N<sub>8</sub>: C, 27.10; H, 2.26; N, 9.03. Found: C, 27.18; H, 2.32; N, 9.15.

### Synthesis of [(bmimb)<sub>2</sub>Cu<sub>4</sub>I<sub>4</sub>]<sub>n</sub> (CP2)

A mixture of CuI (38 mg, 0.2 mmol), bmimb (21.3mg, 0.08 mmol), and CH<sub>3</sub>CN (2 mL), H<sub>2</sub>O (6 mL) was sealed in a 15 mL Teflon-lined autoclave, which was heated at 180 °C for 3 days. After slowly cooling to RT, the colorless block crystals suitable for X-ray diffraction analysis were obtained, which was washed with distilled water and acetonitrile several times, and finally dried in air. Yield: 62%. 669(w), 685(w), 729(s), 758(s), 776(w), 826(w), 848(w), 970(w), 1000(w), 1070(w), 1140(s), 1150(s), 1280(s), 1350(m), 1360(w), 1430(s), 1450(w), 1480(s), 1500(s), 1540(s), 1700(s). Anal. Calcd for C<sub>32</sub>H<sub>36</sub>Cu<sub>4</sub>I<sub>4</sub>N<sub>8</sub>: C, 29.63; H, 2.78; N, 8.64. Found: C, 29.88; H, 2.74; N, 8.68.

## Spectroscopic Measurements

<sup>1</sup>H NMR analyses were performed on a Bruker Avance III HD-600 MHz spectrometer. The IR spectra of polycrystalline solids were recorded on a Nicolet Magna-IR750 spectrophotometer in the 4000–400 cm<sup>-1</sup> region (w, weak; b, broad; m, medium; s, strong) by KBr disc. Solid-state

UV-vis spectra were recorded on a SHIMADZU UV-3600 spectrophotometer. Powder X-ray diffraction (PXRD) patterns were recorded on a RINT2000 vertical goniometer with CuK $\alpha$  X-ray source (operated at 40 kV and 100 mA). Elemental analyses (C, H, and N) were conducted with a Perkin Elmer 2400 analyzer. Simulations of the PXRD patterns were calculated with CrystalDiffract using crystal structure parameters analyzed by single-crystal X-ray crystallography (Copyright©2015 Crystal Maker Software Ltd). Photoluminescence (PL) spectra were recorded on an Edinburgh FS5 model instrument. The slit width was fixed at 0.2 nm for both excitation and emission light. PL Emission and excitation spectra were corrected for the spectral response of the monochromator and the detector, using typical correction spectra provided by the manufacturer. The PL measurements at low temperatures were performed using a liquid N<sub>2</sub> closed-cycle cryostat. The absolute emission quantum yield (QY) values were measured at RT using an Edinburgh quantum yield measurement system, equipped with a 150 W xenon lamp coupled to a monochromator for wavelength discrimination, an integrating sphere as the sample chamber, and a multichannel analyzer for signal detection. PL decays were recorded using an Edinburgh FLS980 steady state fluorimeter with a time-correlated single-photon counting (TCSPC) spectrometer and a pulsed xenon lamp as the excitation source.

### **Crystal Structure Determination**

The X-ray diffraction intensity data of complexes **CP1** and **CP2** at 100 K were collected on a Bruker APEX-2 CCD with graphite-monochromated MoK $\alpha$  radiation ( $\lambda=0.71073\text{\AA}$ ).<sup>2</sup> Data collection, data reduction, and cell refinement were performed with the Bruker Instrument Servicev 4.2.2 and SAINTV 8.34A software.<sup>3,4</sup> Structures were solved by direct methods using the SHELXS program, and refinement was performed using SHELXL based on  $F^2$  through full-matrix least-squares routine.<sup>5</sup> Absorption corrections were applied with multi-scan program SADABS.<sup>6</sup> Hydrogen atoms of organic ligands were generated geometrically by the riding mode, and all the non-hydrogen atoms were refined anisotropically through full-matrix least-squares technique on  $F^2$  with the SHELXTL program package.<sup>7</sup> The crystallographic data and refinement parameters is summarized in Table S2. Selected bond lengths for **CP1** and **CP2** are listed in Table S3 and S4. Crystallographic data for the structures reported in this paper have been deposited with the Cambridge Crystallographic Data Centre (CCDC No. 2214797-2214798).

### **Solid-state NMR at Variable Temperatures**

The solid-state NMR experiments were performed at the field of 9.4 Tesla on a Bruker AVANCE III 400 MHz spectrometer. The <sup>13</sup>C signals were acquired at the resonance frequency of 100.63 MHz using a 7 mm double-resonance probe. The magic angle spinning rate was set to 5 kHz. As for the <sup>1</sup>H→<sup>13</sup>C CPTOSS NMR experiments, the contact time was 2.0 ms and the repetition time was 8.0 s. The <sup>13</sup>C chemical shifts were referenced to tetramethylsilane (TMS) and glycine (a second reference to TMS). The temperature was controlled by a Bruker temperature controller with a deviation of  $\pm 1.0$  K. Above RT (RT), the temperature was changed in 5 K/min intervals and a 90 min period was sufficient to allow temperature stabilization before collecting the data.

### **Temperature-Dependent Raman Spectra**

Raman spectra were recorded with LabRam HR Evolution confocal Raman microscopy (Horiba). The excitation laser was an air-cooled intra-cavity regulated laser diode with point source for maximal confocal performance (785 nm/17 mw). The objective was 50× and numerical aperture (NA) was 0.50. The Raman scattered light was dispersed by a spectrometer with a 600 grooves/mm grating. A nitrogen microscopy cryostat (THCELL-600, Linkam Scientific Instruments, Inc.) equipped with a controller was used to control the temperature.

### **Temperature-Dependent Ultrafast Transient Absorption Spectroscopy**

The femtosecond time-resolved transient absorption (fs-TA) measurements were performed on an EOS pump-probe system (Ultrafast Systems LLC) in combination with an amplified femtosecond laser system (Coherent). The pump pulses (~50 μW at the sample) were delivered by an optical parametric amplifier (TOPAS-800-fs), which excited by a Ti:sapphire regenerative amplifier (Legend Elite-1K-HE; center wavelength 800 nm, pulse duration 35 fs, pulse energy 3 mJ, repetition rate 1 kHz) seeded with a mode-locked Ti:sapphire laser system (Micra 5). The white-light-continuum (WLC) probe pulses (500-750 nm) was generated by focusing a picosecond Nd:YAG laser beam into a photonic crystal fiber. The time delays (from 8 ns up to 100 μs) between the pump and probe pulses were controlled by a digital delay generator. The instrument response function (IRF) was determined to be ~100 ps. The temporal and spectral profiles (chirp-corrected) of the pump-induced differential transmission of the WLC probe light were visualized by an optical fiber-coupled multichannel spectrometer (with a CMOS sensor) and further processed by the Surface Xplorer software. The samples sandwiched between two 1-mm-thick quartz plates were placed in an Oxford Instrument temperature controller (78–498 K).

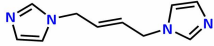
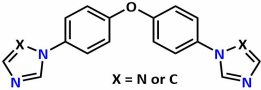
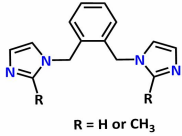
### **Thermogravimetric Analysis**

Thermogravimetric analyses were performed on the Labsys Evo thermal gravimetric analyzer under the atmosphere of nitrogen. About 5 mg of samples were loaded onto a platinum sample pan and heated from RT to 850 °C at a rate of 10 °C/min. The TGA diagrams of **CP1** and **CP2** are shown in Fig. S3.

### **LED Devices Fabrication**

The well-stirred mixture of stoichiometric **CP1** or **CP2** and pouring sealant (ZWL8820) was firstly deaerated in vacuum oven at RT. A commercial Epileds InGaN LED chip with an emission wavelength of ca. 365 nm was covered by the mixture with the forward bias current of the LEDs in the range of 10–400 mA. The electroluminescence (EL) spectra of the LEDs at RT was recorded with an Everfine HAAS-2000 equipment.<sup>8</sup> In the spectral measurements, an integrating sphere (a diameter of 30 cm) was coupled to a high-accuracy array spectroradiometer (wavelength accuracy < 0.3 nm) and a programmable test power LED 300E.<sup>9</sup> For fabrication of white pc-wLED, a UV LED chip was integrated with the three-component mixture containing commercial blue phosphor (BAM:Eu<sup>2+</sup>), green phosphor (Ba,Sr)<sub>2</sub>SiO<sub>4</sub>:Eu<sup>2+</sup> and **CP1** or **CP2** phosphors with the weight ratio of ca. 2:1:1.<sup>10</sup>

**Table S1** The imidazole-terminal ligands for synthesis of NTQ molecular-based materials.

Ligand	CP	NTQ temp. region	Ref.
 $\xrightarrow[\text{MeCN/H}_2\text{O}]{\text{CuI}}$ 150 °C, 3 days	[bibeCu <sub>4</sub> I <sub>4</sub> ] <sub>n</sub>	78–260 K	Year 2020
 $\xrightarrow[\text{MeCN/H}_2\text{O}]{\text{CuI}}$ 150 °C, 4 days	[bidpeCu <sub>2</sub> I <sub>2</sub> ] <sub>n</sub> [btdpeCu <sub>2</sub> I <sub>2</sub> ] <sub>n</sub>	78–238 K TQ	Year 2021
 $\xrightarrow[\text{MeCN/H}_2\text{O}]{\text{CuI}}$ 180 °C, 3 days	[(bimb) <sub>2</sub> Cu <sub>4</sub> I <sub>4</sub> ] <sub>n</sub> [(bmimb) <sub>2</sub> Cu <sub>4</sub> I <sub>4</sub> ] <sub>n</sub>	372–462 K 385–475 K	This work

Reference note:

1. T. Wu, S. Jiang, P. N. Samanta, Y. Xie, J. Li, X. Wang, M. Devashis, X. Gu, Y. Wang, W. Huang, Q. Zhang, J. Leszczynski and D. Wu, *Chem. Commun.*, 2020, **56**, 12057–12060.
2. M. Li, Z. Cheng, X. Wang, Z. Yu, M. Zhou, H. Miao, W. Zhaxi, W. Huang, X. Ma, Q. Chen, S. Jiang, Q. Zhang and D. Wu, *J. Phys. Chem. Lett.*, 2021, **12**, 8237–8245.

**Table S2** The structural parameters of **CP1** and **CP2**.

Formula	<b>C<sub>28</sub>H<sub>28</sub>Cu<sub>4</sub>I<sub>4</sub>N<sub>8</sub></b>	<b>C<sub>32</sub>H<sub>36</sub>Cu<sub>4</sub>I<sub>4</sub>N<sub>8</sub></b>
Temperature (K)	100	100
Wavelength (Å)	0.71073	0.71073
Formula weight	1238.34	1294.45
Crystal system	triclinic	monoclinic
Space group	$P\bar{1}$	$P2_1/c$
<i>a</i> [Å]	8.7406(3)	8.9276(2)
<i>b</i> [Å]	10.0825(3)	14.0857(4)
<i>c</i> [Å]	20.1649(6)	29.8293(8)
$\alpha$ [°]	85.02	90
$\beta$ [°]	81.294(2)	90.860(2)
$\gamma$ [°]	81.294(2)	90
<i>V</i> [Å <sup>3</sup> ]	1732.64(9)	3750.66(17)
<i>Z</i>	2	4
$\rho_{\text{calcd}}$ [g/cm <sup>3</sup> ]	2.374	2.292
<i>F</i> (000)	1160	2448
$R_1^a/wR_2^b[I > 2\sigma(I)]$	0.0453/ 0.1077	0.0768/0.1809
$R_1/wR_2$ (all data)	0.0697/0.1225	0.0843/0.1848
<i>GOF</i> <sup>c</sup> on <i>F</i> <sup>2</sup>	1.019	1.025

$$^a R_1 = \Sigma(|F_0| - |F_c|) / \Sigma|F_0|; \quad ^b wR_2 = [\Sigma w(|F_0|^2 - |F_c|^2)^2 / \Sigma w|F_0|^2]^{1/2};$$

$$^c \text{GOF} = [\Sigma[w(F_0^2 - F_c^2)^2] / (N_{\text{obs}} - N_{\text{params}})]^{1/2}, \text{ based on the data } I > 2\sigma(I).$$

**Table S3** The selected bond distances (Å) for **CPI** at 100 K.

---

Cu1 I1	2.8434(13)	C14 N4	1.391(11)
Cu2 I1	2.6078(13)	C15 N5	1.313(12)
Cu4 I1	2.6678(12)	C16 N5	1.386(11)
Cu1 I2	2.6273(13)	C15 N6	1.348(13)
Cu2 I2	2.9189(13)	C17 N6	1.400(12)
Cu3 I2	2.6746(12)	C18 N6	1.447(12)
Cu2 I3	2.7019(12)	C25 N7	1.454(12)
Cu3 I3	2.8212(12)	C26 N7	1.359(12)
Cu4 I3	2.6244(13)	C27 N7	1.389(11)
Cu1 I4	2.6776(12)	C26 N8	1.318(12)
Cu3 I4	2.6520(13)	C28 N8	1.375(10)
Cu4 I4	2.9156(13)	C2 C3	1.350(14)
Cu2 Cu1	2.7469(16)	C4 C5	1.510(13)
Cu3 Cu1	2.5252(14)	C5 C6	1.373(14)
Cu1 Cu4	2.6654(15)	C5 C10	1.386(14)
Cu1 N1	1.998(8)	C6 C7	1.383(16)

Cu2 Cu3	2.6401(15)	C7 C8	1.388(15)
Cu2 Cu4	2.5273(14)	C8 C9	1.382(15)
Cu2 N5	1.983(7)	C9 C10	1.395(13)
Cu3 Cu4	2.7096(16)	C10 C11	1.508(14)
Cu3 N8	1.982(7)	C13 C14	1.341(14)
Cu4 N4	1.965(8)	C16 C17	1.347(13)
C1 N1	1.288(12)	C18 C19	1.515(12)
C2 N1	1.388(11)	C19 C20	1.419(13)
C1 N2	1.360(12)	C19 C24	1.377(14)
C3 N2	1.372(12)	C20 C21	1.379(14)
C4 N2	1.472(13)	C21 C22	1.369(14)
C11 N3	1.454(13)	C22 C23	1.417(13)
C12 N3	1.357(12)	C23 C24	1.393(13)
C13 N3	1.388(12)	C24 C25	1.526(13)
C12 N4	1.340(12)	C27 C28	1.359(12)

---

**Table S4** The selected bond distances (Å) for **CP2** at 100 K.

---

Cu1 Cu2	2.655(2)	C1 C2	1.494(15)
Cu1 Cu3	2.557(3)	C2 N1	1.323(14)
Cu1 I1	2.889(3)	C2 N2	1.336(14)
Cu1 I2	2.654(2)	Cu3 N1	1.973(12)
Cu1 I3	2.652(3)	C3 C4	1.316(16)
Cu1 N4	1.994(10)	C3 N2	1.383(14)
Cu2 Cu4	2.553(2)	C5 C6	1.512(14)
Cu2 I1	2.624(2)	C4 N1	1.400(15)
Cu2 I2	2.864(2)	C5 N2	1.455(13)
Cu2 I4	2.6398(19)	C6 C7	1.397(15)
Cu2 N4	2.004(11)	C6 C11	1.415(14)
Cu3 Cu4	2.738(3)	C7 C8	1.375(16)
Cu3 I2	2.631(2)	C8 C9	1.389(15)
Cu3 I3	2.563(3)	C9 C10	1.393(15)
Cu4 I1	2.623(2)	C10 C11	1.382(14)

---

**Table S5** The PL properties of the Cu(I)-containing NIR emitters.

No.	Compound	PLE peak (nm)	PL peak (nm)	FWHM (nm)	PLQY (%)	$\tau$ ( $\mu$ s)	$K_r$ / $10^4\text{s}^{-1c}$	$K_{nr}$ / $10^4\text{s}^{-1d}$	Ref.
1	[CuI <sub>3</sub> (pymt) <sub>3</sub> ] <sub>n</sub>	462	752	150	n.d.	4.06	-	-	[1]
2	Cu <sub>6</sub> (btt) <sub>6</sub>	371	861	200	n.d.	7.41	-	-	[2]
3	[CuI <sub>3</sub> (4-ptt) <sub>3</sub> ] <sub>2</sub> ·3DMF·3H <sub>2</sub> O	390	904	440	4.3	13.9	0.31	6.88	[3]
	[CuI (4-ptt)] <sub>6</sub> ·8DMF·7H <sub>2</sub> O	460	776	250	1.6	2.88	0.56	34.7	
4	[(CuI <sub>4</sub> I <sub>4</sub> ) <sub>3</sub> (CuI <sub>6</sub> ) <sub>2</sub> (3-ptt) <sub>12</sub> ] <sub>n</sub> ·24nDEF·12nH <sub>2</sub> O	275	785	50	1.72	-	-	-	[4]
		370	795	50	n.d.	-	-	-	
5	[Cu <sub>4</sub> (I) <sub>4</sub> (PPh <sub>3</sub> ) <sub>4</sub> ]	390	711 <sup>f</sup>	150	n.d.	7.7	-	-	[5]
	[Cu(pybt)(PMe <sub>3</sub> ) <sub>2</sub> ] <sub>2</sub> PF <sub>6</sub>	n.d.	752	250	1 <sup>e</sup>	0.8	1.2	123.75	
6	[Cu(qybt)(PMe <sub>3</sub> ) <sub>2</sub> ] <sub>2</sub> PF <sub>6</sub>	n.d.	724	210	1 <sup>e</sup>	0.6	1.67	165	[6]
	[Cu(pybt)(dppe)]PF <sub>6</sub>	n.d.	653	200	1 <sup>e</sup>	0.8	1.25	123.75	
	[Cu(qybt)(dppe)]PF <sub>6</sub>	n.d.	727	220	1 <sup>e</sup>	n.d.	-	-	
	[Cu(pybt)(IDipp)]PF <sub>6</sub>	n.d.	683	200	2	0.6	3.33	163	
7	B <sub>2</sub> IDip <sub>2</sub>	385	<i>a</i>	n.d.	<i>a</i>	<i>a</i>	-	-	[7]
	[B <sub>2</sub> (IDip) <sub>2</sub> {Cu(C <sub>2</sub> SiMe <sub>3</sub> ) <sub>2</sub> }] <sub>2</sub>	480	805	220	<i>a</i>	<i>a</i>	-	-	
8	[B <sub>2</sub> (IDip) <sub>2</sub> (CuCl) <sub>2</sub> ]	420	805	200	3	25	0.12	3.88	[8]
	[Cu <sub>11</sub> (TBBT) <sub>9</sub> (PPh <sub>3</sub> ) <sub>6</sub> ](SbF <sub>6</sub> ) <sub>2</sub>	450	675	100	22	1.3	16.92	60	
9	Rb <sub>6</sub> (C <sub>4</sub> H <sub>8</sub> OS) <sub>12</sub> [Cu <sub>8</sub> Cl <sub>13</sub> ][Cu <sub>4</sub> Cl <sub>4</sub> (OH)(H <sub>2</sub> O)]	348	732	234	2.9	3.95	0.73	2.46	[9]
	K <sub>6</sub> (C <sub>4</sub> H <sub>8</sub> OS) <sub>12</sub> [Cu <sub>8</sub> Cl <sub>13</sub> ][Cu <sub>4</sub> Cl <sub>4</sub> (OH)(H <sub>2</sub> O)]	342	722	214	2.6	3.37	0.7	2.61	

	$\text{K}_6(\text{C}_4\text{H}_8\text{OS})_{12}[\text{Cu}_8\text{Br}_{13}][\text{Cu}_4\text{Br}_4(\text{OH})(\text{H}_2\text{O})]$	350	678	158	37	32.28	1.15	1.95	
	$\text{Rb}_6(\text{C}_4\text{H}_8\text{OS})_{12}[\text{Cu}_8\text{Br}_{13}][\text{Cu}_4\text{Br}_4(\text{OH})(\text{H}_2\text{O})]$	370	674	155	42.3	35.21	1.2	1.64	
	$\text{Cs}_6(\text{C}_4\text{H}_8\text{OS})_{12}[\text{Cu}_8\text{Br}_{13}][\text{Cu}_4\text{Br}_4(\text{OH})(\text{H}_2\text{O})]$	383	676	161	41.2	26.39	1.56	22.3	
	$\text{K}_6(\text{DMSO})_{12}[\text{Cu}_8\text{Br}_{13}][\text{Cu}_4\text{Br}_4(\text{OH})(\text{H}_2\text{O})]$	382	678	155	4.6	-	-	-	
	$\text{Rb}_6(\text{DMSO})_{12}[\text{Cu}_8\text{Br}_{13}][\text{Cu}_4\text{Br}_4(\text{OH})(\text{H}_2\text{O})]$	396	688	166	10	-	-	-	
10	$[\text{Cu}(\text{dbm})(\text{CAAC}^{\text{Me}})]$	n.d.	762	260	<i>a</i>	<i>a</i>	-	-	[10]
	$[\text{Cu}(\text{nacnac})(\text{CAAC}^{\text{Me}})]$	n.d.	739	260	<i>a</i>	<i>a</i>	-	-	
11	$(\text{bimb})_2\text{Cu}_4\text{I}_4$	400	650	148	55.23	12.6	4.38	3.55	This
	$(\text{bmimb})_2\text{Cu}_4\text{I}_4$	400	710	145	25.71	11.2	2.3	6.63	wok

[a] Emission too weak. [b] n.d. = not determined. [c] Radiative rate constant calculated  $k_r = \phi / \tau$ . [d] Nonradiative rate constant calculated  $k_{nr} = 1 - \phi / \tau$ . [e] Quantum efficiency of less than 1% is approximate equal to 1%. [f] The PL was measured at 77 K. pynt = pyrimidine-2-thiolate; 4-Hptt = 5-(pyridin-4-yl)-1H-1,2,4-triazole-3-thiol, DMF = N, N-dimethylformamide; Hbtt = 2-benzothiazolethiol; IDip = 1,3-bis(2,6-diisopropylphenyl)imidazole-2-ylidene; (TBBT = 4-tert-butylbenzenethiol); bimb = 1,2-bis((1H-imidazol-1-yl)methyl)benzene; bmimb = 1,2-bis((2-methyl-1H-imidazol-1-yl)methyl)-benzene;

References note: [1] *Chem. Commun.*, **2004**, 21, 2578–2579; [2] *Inorg. Chem.* **2009**, 48, 2873–2879; [3] *Dalton Trans.*, **2012**, 41, 9411–9416; [4] *Chem. Sci.*, **2013**, 4, 1484–1489; [5] *Inorg. Chem.* **2016**, 55, 3206–3208; [6] *Inorg. Chem.* **2017**, 56, 8996–9008; [7] *J. Am. Chem. Soc.* **2017**, 139, 4887–4893; [8] *J. Phys. Chem. Lett.* **2020**, 11, 4891–4896; [9] *Inorg. Chem.* **2022**, 61, 10950–10956; [10] *Inorg. Chem.* **2022**, 61, 14833–14844.

**Table S6** The EL parameters of CP1-based white-light LED at different currents.

<b><i>I</i> (mA)</b>	<b>100</b>	<b>200</b>	<b>300</b>	<b>400</b>
CIE x	0.3443	0.3439	0.3498	0.3511
CIE y	0.3609	0.366	0.3656	0.351
CCT[K]	5058	5090	4880	4772
R1	86.4	87.9	75.9	88.1
R2	90.5	89.1	80.7	89.5
R3	94.2	90.2	83.5	92
R4	91.8	91.7	91.5	90.2
R5	91.2	95.9	90.9	88.8
R6	88.4	95.7	82.1	86.9
R7	87	91	71.8	91.4
R8	82	86.7	68.6	87.9
R9	60.7	73.2	64.6	66.9
R10	79.2	78.7	68.2	76.7
R11	90	95	96.3	90
R12	87.2	87.3	93.4	80.7
R13	86.6	85.9	73.3	87.4
R14	96.9	94.2	90.2	95.6
R15	85.9	87.2	77.4	87
Ra	89	91	80.6	89.3

**Table S7** The EL parameters of CP2-based white-light LED at different currents.

<b><i>I</i> (mA)</b>	<b>10</b>	<b>20</b>	<b>30</b>	<b>40</b>	<b>50</b>	<b>60</b>	<b>70</b>	<b>80</b>	<b>90</b>	<b>100</b>	<b>110</b>	<b>120</b>	<b>130</b>	<b>140</b>	<b>150</b>	<b>160</b>	<b>170</b>	<b>180</b>	<b>190</b>	<b>200</b>
CIE x	0.33	0.34	0.35	0.35	0.35	0.35	0.35	0.35	0.34	0.34	0.34	0.34	0.33	0.33	0.33	0.33	0.33	0.32	0.32	0.32
CIE y	0.37	0.36	0.37	0.37	0.37	0.37	0.37	0.37	0.37	0.37	0.37	0.37	0.37	0.37	0.37	0.36	0.36	0.36	0.36	0.36
CCT[K]	5452	4965	4821	4864	4706	4751	4779	4852	4924	4999	5092	5188	5285	5381	5425	5551	5602	5671	5753	5825
R1	97.9	89.3	94.8	98.5	93.6	98.9	98	98.5	98.2	96.6	97	96.4	96.4	95.9	91.9	93.6	91.1	89.2	89.8	89
R2	96.4	89.3	93.9	97.4	93.1	96.9	96.4	96.7	96.7	95.5	96.2	95.8	95.9	95.6	92.4	94.2	92.1	90.8	91.3	91
R3	96.2	90.1	94.1	97.9	92.6	97.3	96.8	97.4	97.5	96.8	97.4	97.4	97.7	97.7	95.7	97.5	96.3	95.8	96.4	96.6
R4	91.9	91.2	93.5	94.5	92.2	94.4	94.5	94.3	94.3	94.2	96.2	95.8	95.1	94.9	94.8	93.9	93.8	94.3	92.6	92.3
R5	93	90.3	94.6	97.5	91.9	97	97	97.1	97.6	97.6	98.3	97.9	97	96.7	96.9	95.6	95.8	96.4	94.5	94.1
R6	94.8	87	93.1	98.4	89.6	97.7	96.8	98.2	98.2	97.6	98.3	98.6	98.3	97.8	98.4	97	98	97.7	97.1	96.7
R7	96.3	83.6	90.3	93.9	87.6	94.6	93.5	94.5	93.7	93	95.3	95.5	96	95.5	94.5	95	94.6	92.7	94.5	94
R8	97.8	84.8	91.5	95.2	89.5	95.9	94.8	95.7	95	94	95.2	95.1	95.4	94.8	91.3	92.9	90.7	88.4	89.4	88.5
R9	93.1	91.7	96.8	97.9	97.6	98.2	98.7	98.7	98.4	96.1	94.1	92.7	91.9	90.6	85.4	85.2	81.8	77.8	77.6	75
R10	94.5	85.6	91.8	95.4	91.1	95.4	94.8	95	94.8	93.3	94.4	93.7	93.8	93.2	89	90.8	88.1	85.8	86.8	86.1
R11	94.3	90.7	93.9	97.3	91.6	96.6	96.3	96.9	97	96.8	97.3	97.3	96.9	96.5	96.5	95	95.2	95	93.7	92.9
R12	82	87.5	85.3	82.7	88.1	83.3	83.7	82.8	82.6	82.4	87.6	86.6	85.6	85.3	84.7	83.7	83	83.2	81.5	81.2

R13	94.8	86.7	92.8	96.5	91.8	96.2	95.8	95.8	96	94.5	95.5	94.9	94.8	94.4	89.9	92.3	89.2	87.5	87.9	87.4
R14	97.4	93.5	96	98.6	95	98.1	97.8	98.2	98.3	98	98.3	98.4	98.6	98.6	97.4	98.6	97.8	97.7	97.9	98.1
R15	94.1	87.7	92.4	95.3	92.5	94.9	94.5	94.4	94.4	93	94.2	93.5	93.3	92.8	88.7	90.4	87.7	85.9	86.1	85.3
Ra	95.5	88.2	93.2	96.7	91.3	96.6	96	96.5	96.4	95.7	96.7	96.6	96.5	96.1	94.5	95	94.1	93.2	93.2	92.8

---

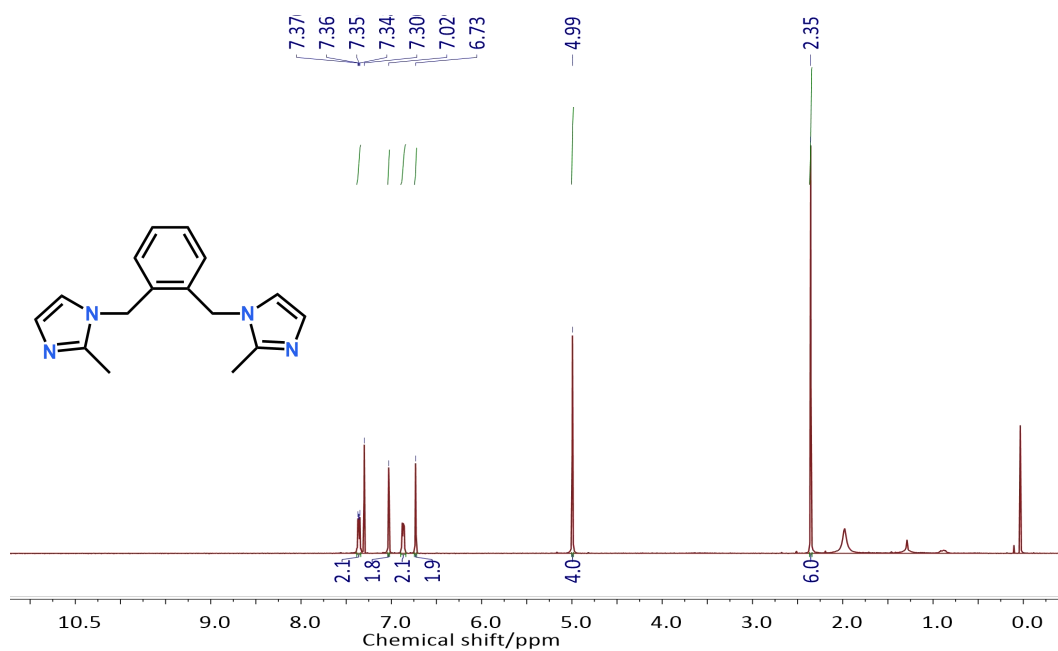
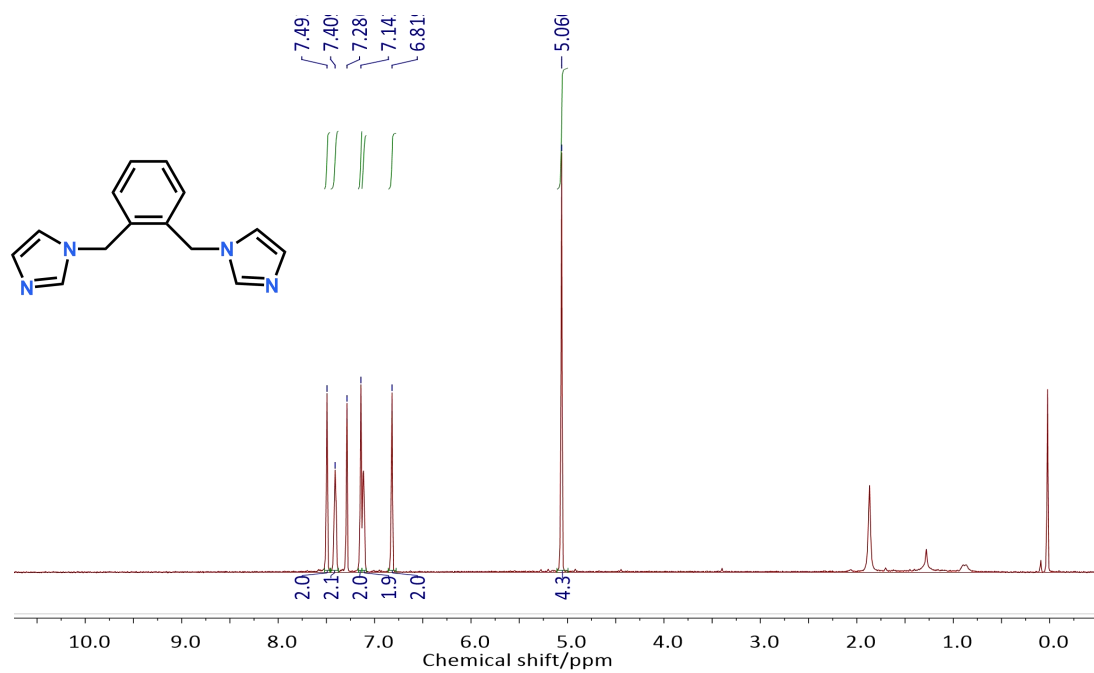


**Fig. S1** <sup>1</sup>H NMR spectrum of the ligands used in this work.

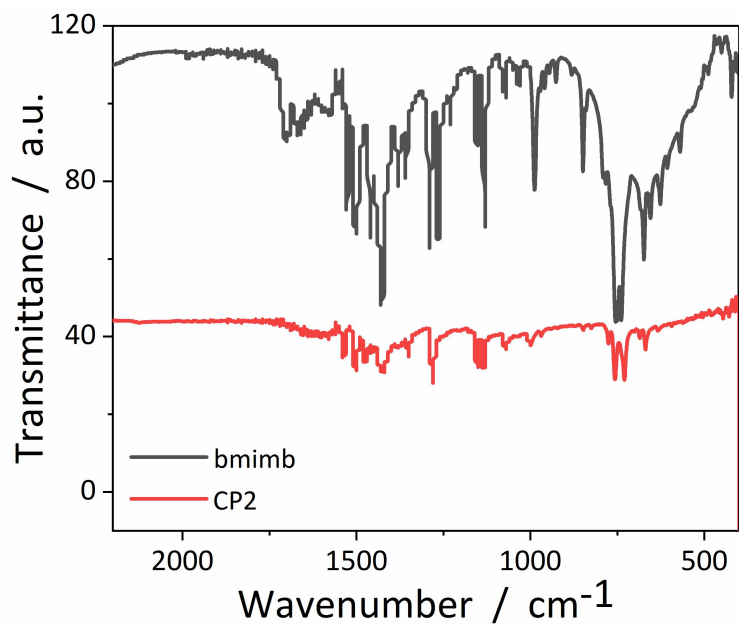
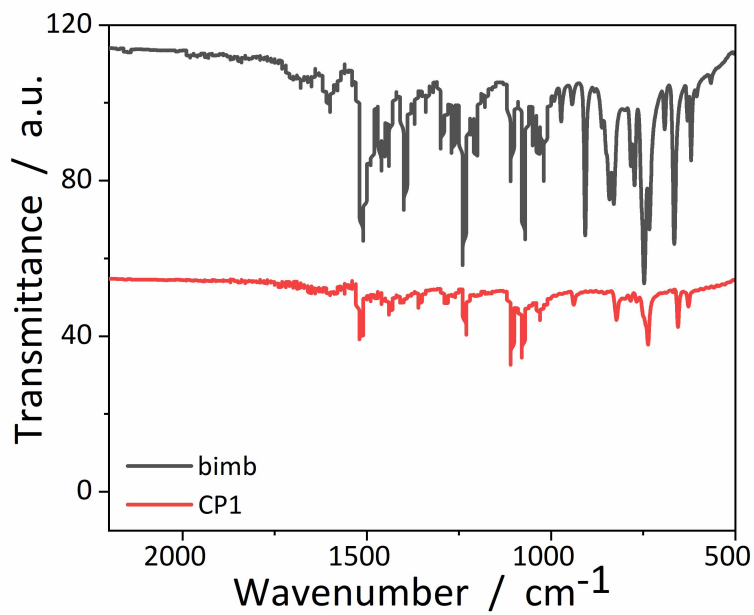


**Fig. S2** The IR spectrum of **CP1** (top) and **CP2** (below) as well as the ligands used.

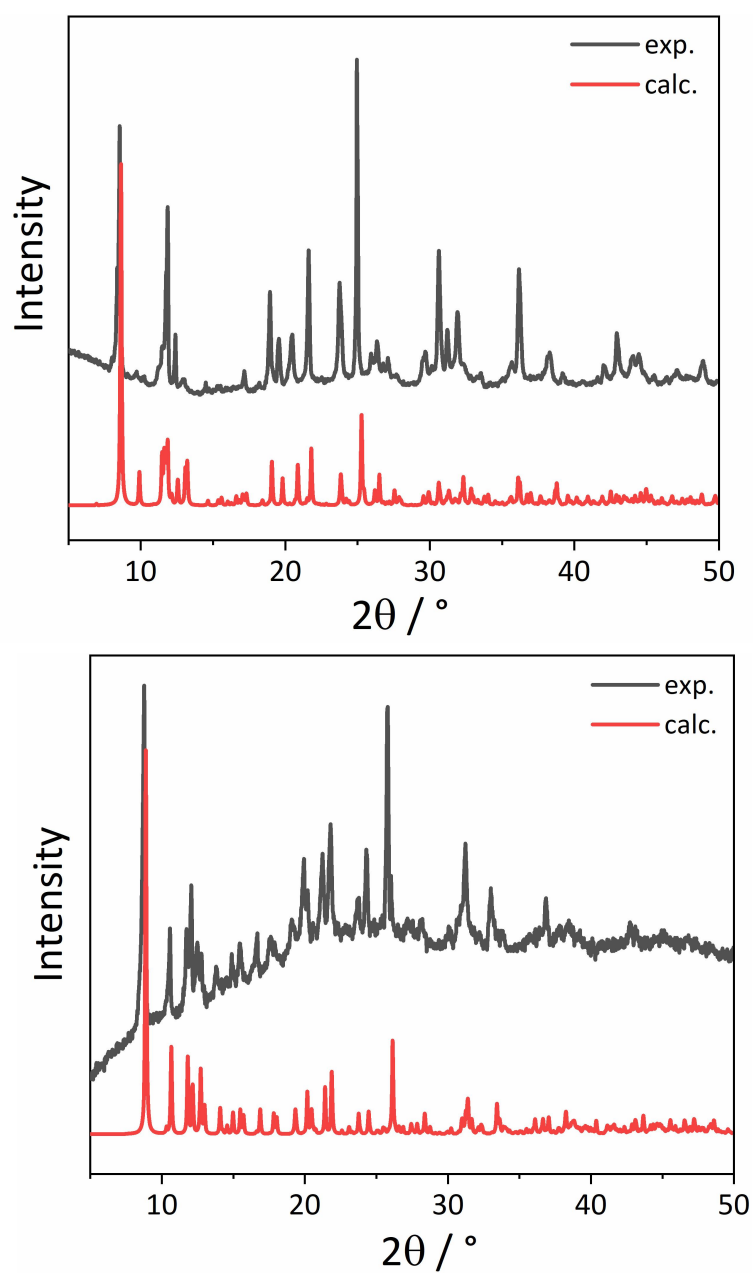
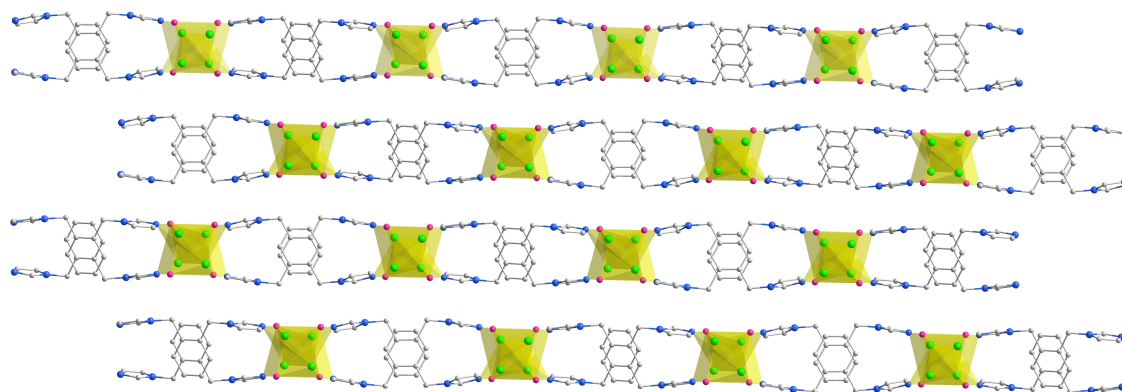


**Fig. S3** The powder XRD patterns of **CP1** (top) and **CP2** (below). The powder XRD patterns match well with the calculated ones from single-crystal X-ray diffraction (SC-XRD) data, indicating the phase purity of bulk crystal.

(a)



(b)

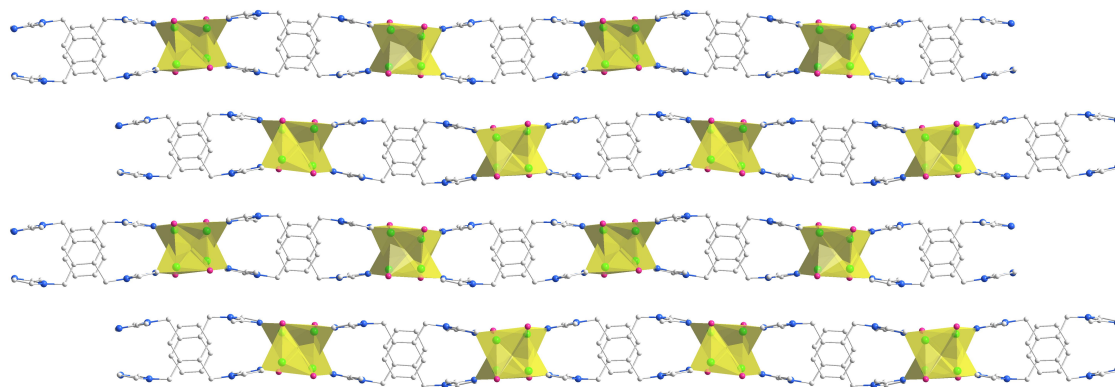


**Fig. S4** Polyhedral representation of 2D structures of **CP1** (a) and **CP2** (b) at 100 K.

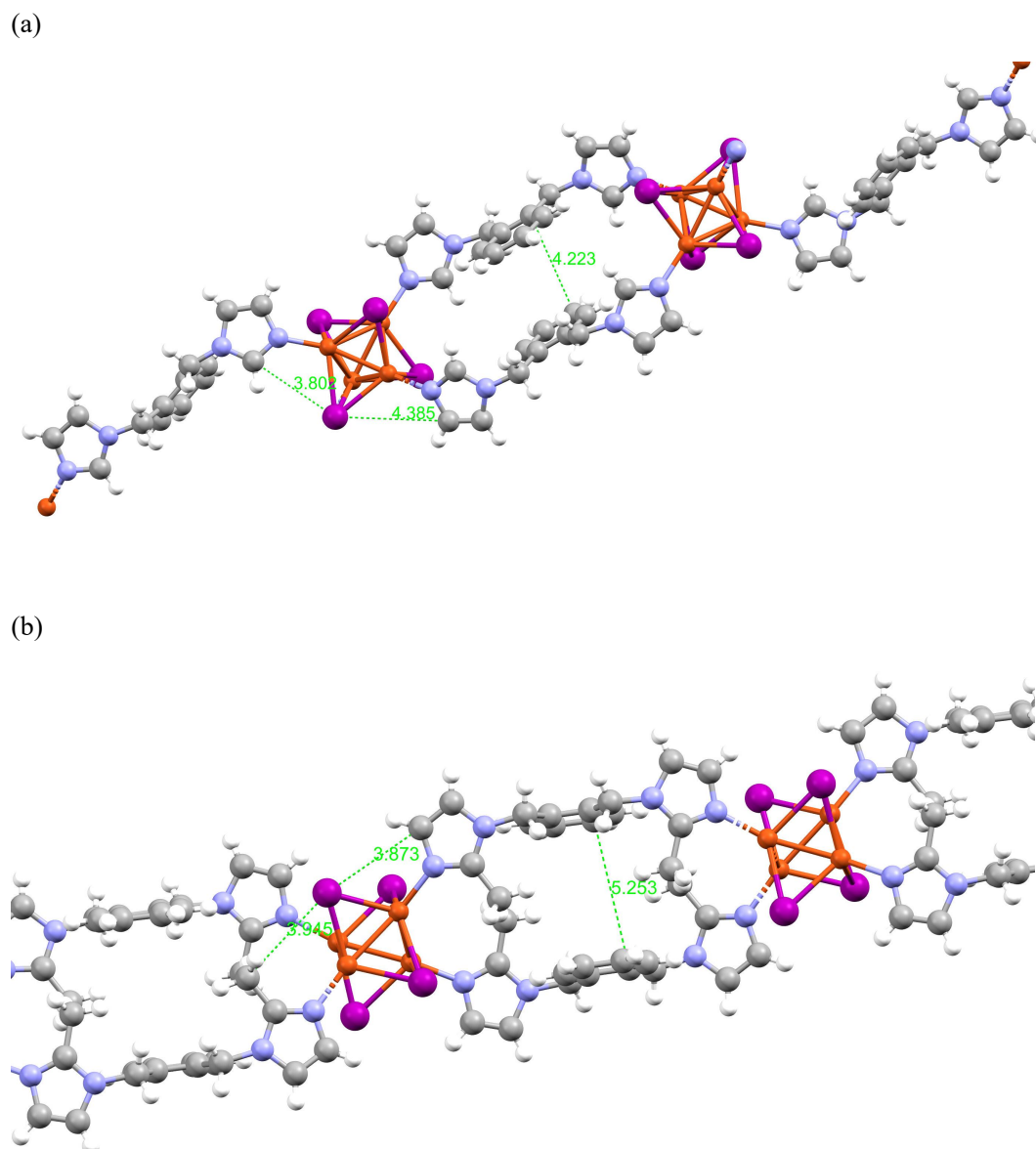
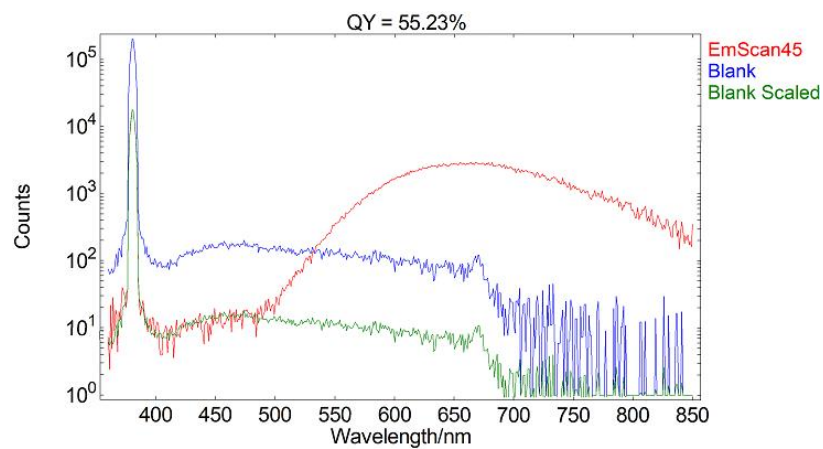


**Fig. S5** The local distances showing the separation of benzene rings and C-H...I interaction in CP1 (a) and CP2 (b). The methyl group also gives rise to the weak C-H...I interaction, which decreases the compactness of Cu<sub>4</sub>I<sub>4</sub> cuboid in CP2. As a consequence, the Cu<sub>4</sub> cuboid shows two long Cu-Cu distances (3.118(3) and 3.284(3) Å) besides four short Cu-Cu distances (2.555(3), 2.556(2), 2.654(3), and 2.737(3) Å) in CP2.

(a)



(b)

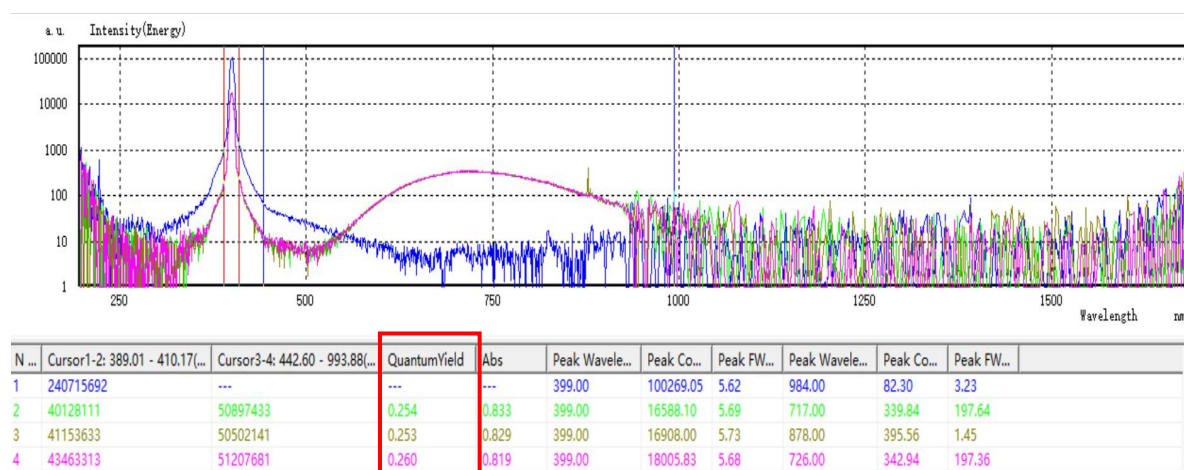


**Fig. S6** The measurements of quantum yield for **CP1** (a) and **CP2** (b).

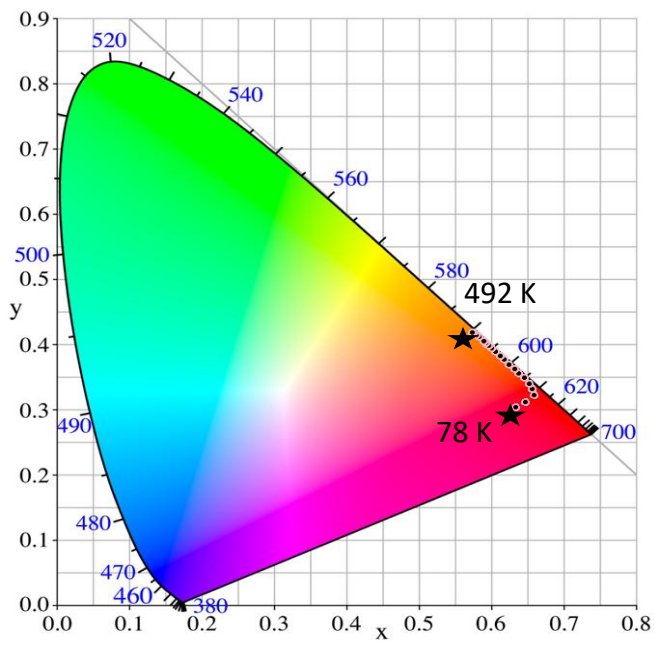


**Fig. S7** Variable temperature CIE diagram of **CPI**.

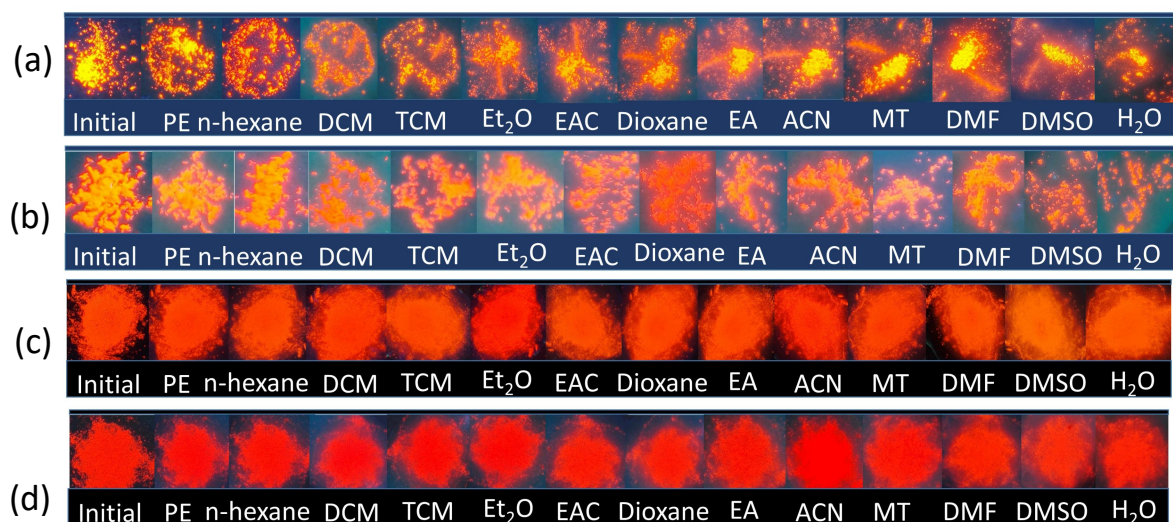


**Fig. S8** Luminescence pictures of **CP1** (a) and **CP2** (b) samples soaked in different organic solvents before grinding. Luminescence pictures of **CP1** (c) and **CP2** (d) samples which are subject to grinding and subsequent soaking in different organic solvents ( $\lambda_{\text{ex}} = 365 \text{ nm}$ ).

The photostabilities of **CP1** and **CP2** samples were investigated through immersing in different organic solvents or being subjected to mechanical grinding, and their PL emissions were not affected by organic solvents or grinding, indicating that the PL can resist chemical or physical stimuli.

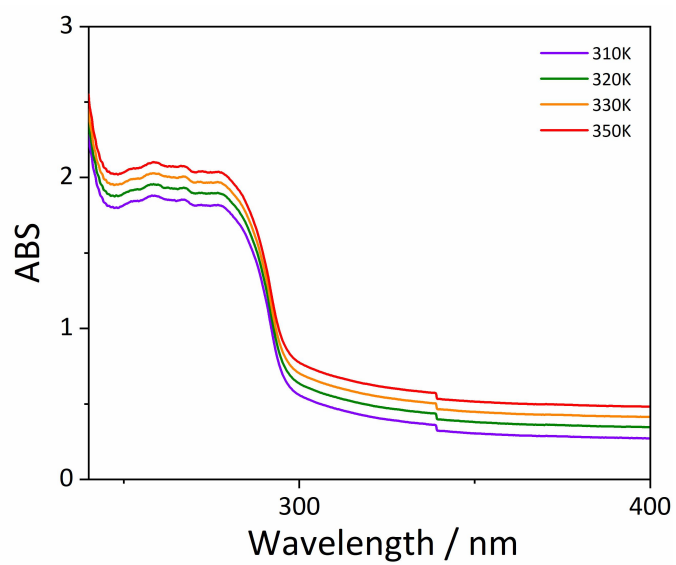
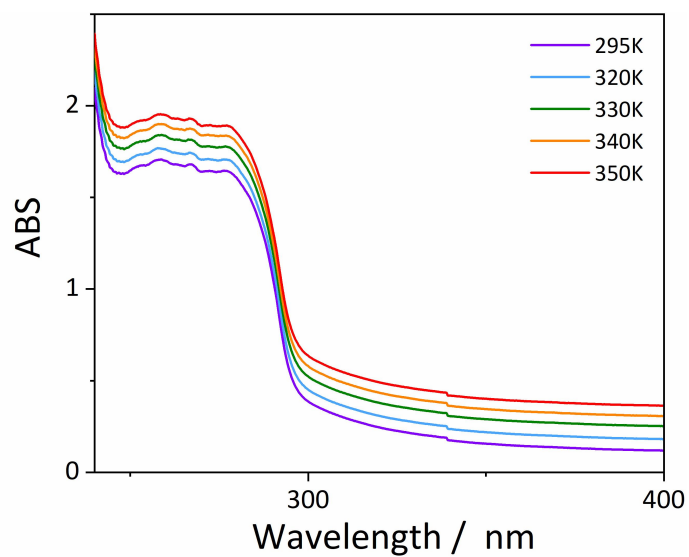


**Fig. S9** The UV-vis absorption spectra of **CP1** (top) and **CP2** (below) at the different temperature.

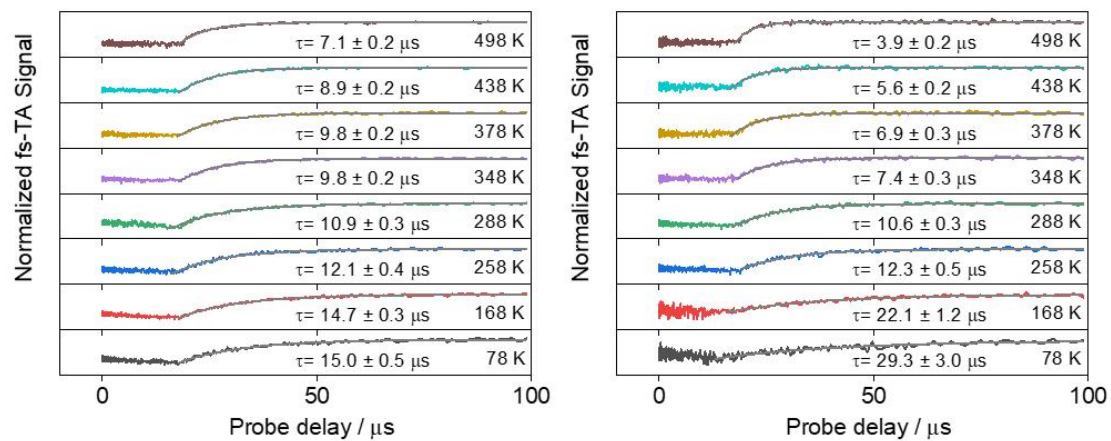


**Fig. S10** The kinetic traces of CP1 (left) and CP2 (right) taken at each peak of the spectral profile at different temperature, respectively. The fs-TA kinetics platform regions suggest an equilibrium relationship between ISC and RISC processes.

To further investigate the TADF mechanism that involve ISC and RISC processes of excited states of the CPs, we performed the femtosecond time-resolved transient absorption (fs-TA) spectroscopy from low to high temperatures. Following the PL emission procedure, the white-light probe (500–750 nm) signals were acquired for samples under the 400 nm pump at different temperatures, as displayed in Fig. S11 a and 11 b. The fs-TA signals of **CP1** and **CP2** exhibit a blue shift with increasing temperature from 78 to 498 K, and the signals continue to gain the intensity at the highest temperature. These results were in good agreement with the PL results. Moreover, these fs-TA kinetic lifetimes show a gradual decrease upon increasing temperature in the temperature range of 78–498 K (Fig. S11 c and 11 d), which is characteristic of the TADF process. Therefore, the above fs-TA spectroscopic characterizations not only evidence the origin of luminescence of CPs but also unravel the temperature-dependent ultrafast dynamics involved.

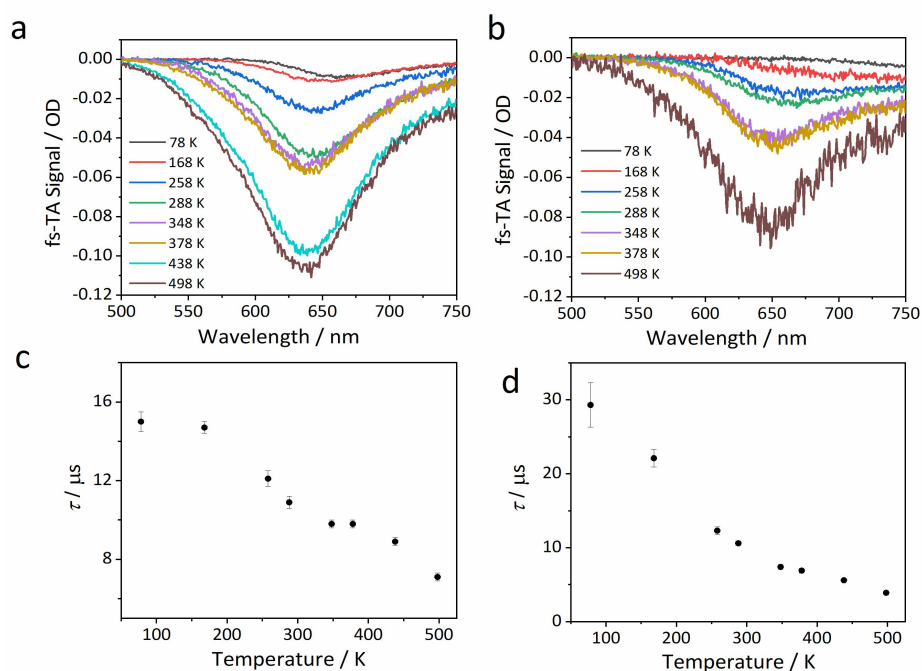


**Fig. S11** Temperature-dependent femtosecond time-resolved transient absorption (fs-TA) spectra of (a) **CP1** and (b) **CP2** at the probe delay of 1  $\mu\text{s}$  under 400 nm excitation. The fs-TA signal (i.e., the absorbance change) is given in optical density (OD). Temperature dependence of the decay times for (c) **CP1** and (d) **CP2**.

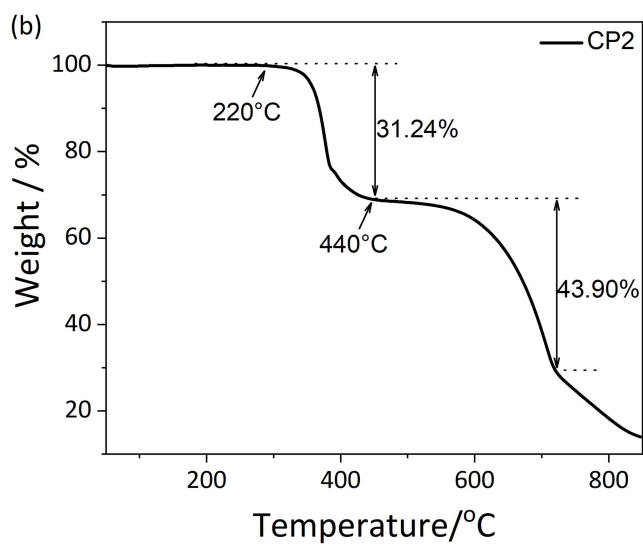
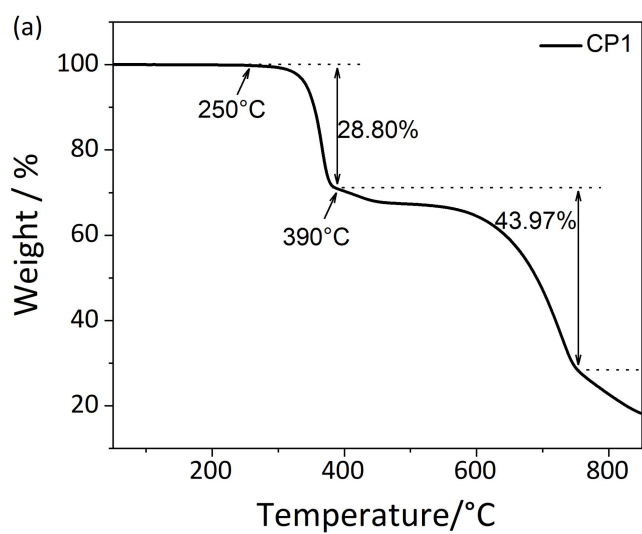


**Fig. S12** The thermogravimetric analysis of **CP1** (a) and **CP2** (b).

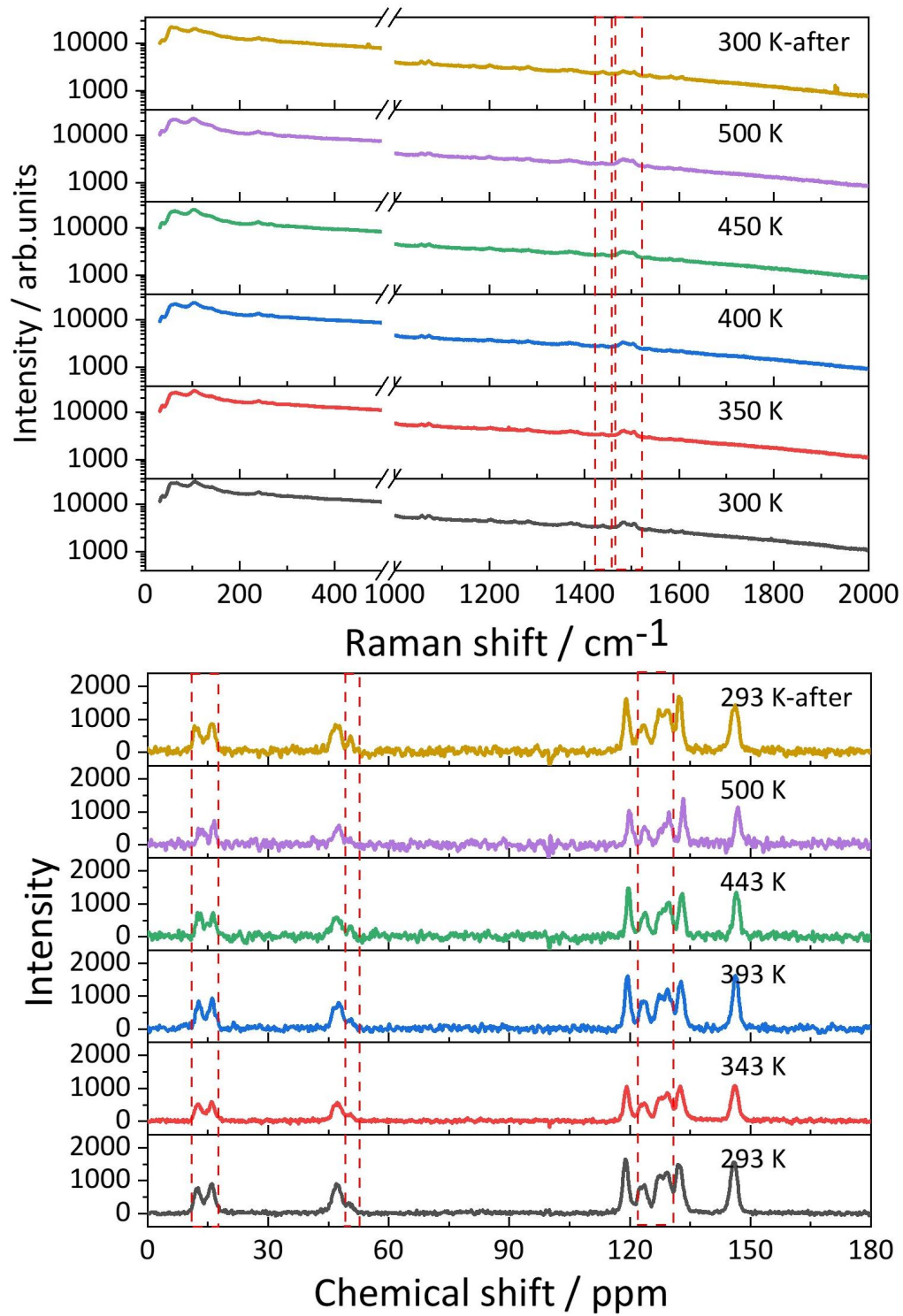


**Fig. S13** Temperature-dependent Raman spectra (top) and <sup>13</sup>C NMR spectra (bottom) of CP2.

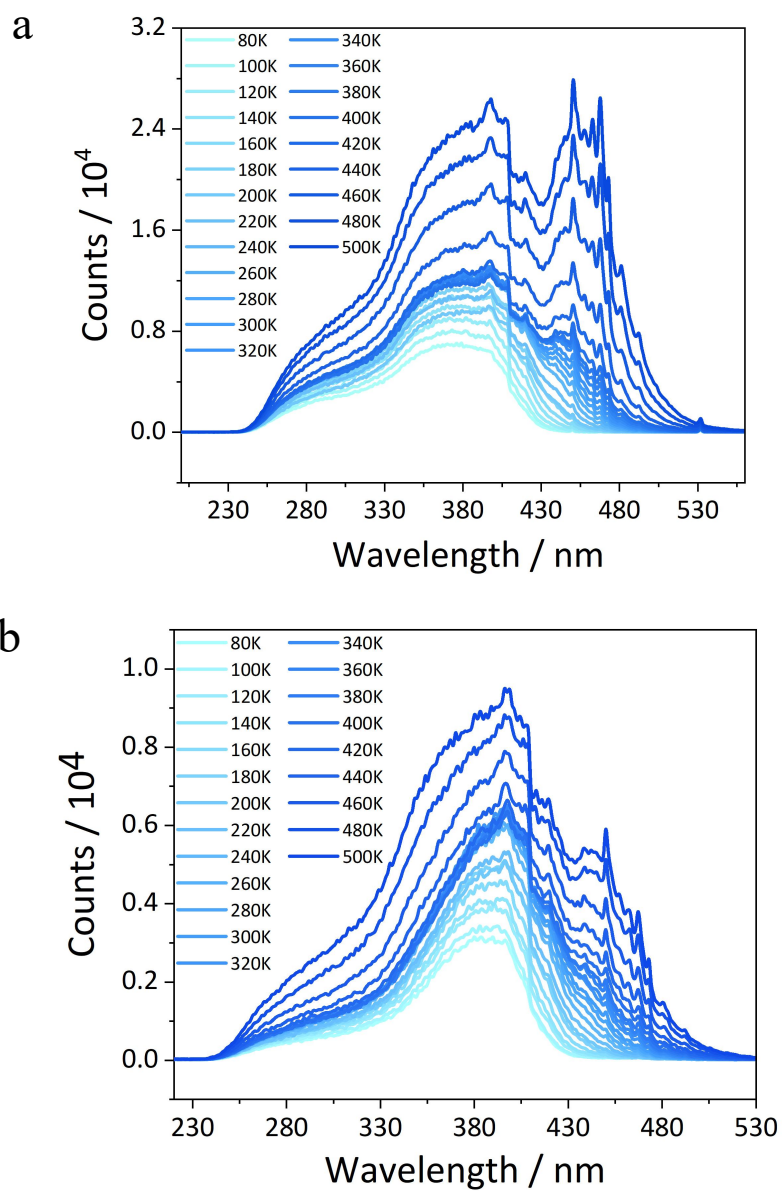


**Fig. S14** Temperature-dependent excitation spectra for **CP1** at  $\lambda_{em} = 650$  nm (a) and **CP2** at  $\lambda_{em} = 710$  nm (b).

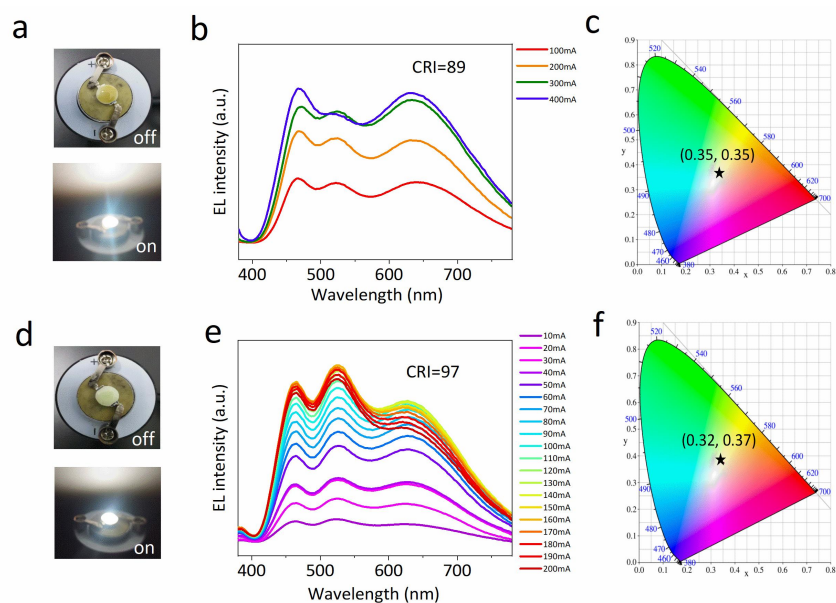


**Fig. S15** (a) Image of **CP1**-based wLED prototype at  $I = 400$  mA. (b) EL spectra of **CP1** wLED with a 365 nm LED chip under a flux operating current of 100–400 mA. (c) The CIE chromaticity coordinates of the wLED in (a). (d) Image of **CP2**-based wLED prototype at  $I = 200$  mA. (e) EL spectra of **CP2** wLED with a 365-nm LED chip under a flux operating current of 10–200 mA. (f) The CIE chromaticity coordinates of the wLED in (d).

## Reference:

- 1 E. Loukopoulos, A. Abdul-Sada, G. Csire, C. Kállay, A. Brookfield, G. J. Tizzard, S. J. Coles, I. N. Lykakis and G. E. Kostakis, *Dalton Trans.*, 2018, **47**, 10491–10508.
- 2 Bruker. SAINT, v8.34A; Bruker AXS Inc: Madison, WI, 2013.
- 3 Bruker APEX2, v2014.5–0; Bruker AXS Inc: Madison, WI, 2007.
- 4 Sheldrick, G. M. *Acta Crystallogr., Sect. A: Found. Crystallogr.* 2008, **A64**, 112.
- 5 Bruker. SADABS, Bruker AXS Inc: Madison, WI, 2014.
- 6 SHELXTL V5.1, Software Reference Manual; Bruker, AXS, Inc: Madison, WI, 1997.
- 7 A. L. Spek, *J Appl Crystallogr.*, 2003, **36**, 7–13.
- 8 X. Geng, Y. Xie, Y. Ma, Y. Liu, J. Luo, J. Wang, R. Yu, B. Deng and W. Zhou, *Journal of Alloys and Compounds*, 2020, **847**, 156249.
- 9 S. Yang, D. Wu, W. Gong, Q. Huang, H. Zhen, Q. Ling and Z. Lin, *Chem. Sci.*, 2018, **9**, 8975–8981.
- 10 C. Ji, T.-H. Huang, Z. Huang, J. Wen, W. Xie, X. Tian, T. Wu, H. He and Y. Peng, *J. Lumin.*, 2019, **216**, 116734.